

---

# Nanosecond solvation dynamics in a polymer electrolyte for lithium batteries

---

In the format provided by the authors and unedited

---

## Supplementary Information

### S1. Synthesis Materials and Methods

**Materials.** All manipulations of air- and water-sensitive compounds were carried out under argon in a glovebox. All chemicals were purchased from commercial sources and used as received: dimethyl malonate (98%), 1,5-pentanediol (purity,  $\geq 97.0\%$  (GC)), titanium(IV) isopropoxide (99.999% trace metals basis) were purchase from MilliporeSigma and used as received. Lithium bis(trifluoromethanesulfonyl)imide (LiTFSI, 99.95% trace metals basis) were purchase from Aldrich and vacuum dried at 90 °C for 3 days before use.

**Instruments.**  $^1\text{H}$  NMR spectra were recorded on a Bruker Avance IV NEO spectrometer with a 5 mm 1H/BB iProbe ( $^1\text{H}$ , 500 MHz) and referenced to the residual chloroform (7.26 ppm) signals.  $^{13}\text{C}$  NMR spectra were recorded on a Bruker Avance IV NEO spectrometer with a 5 mm 1H/BB iProbe ( $^{13}\text{C}$ , 126 MHz) and referenced to the residual chloroform (77.16 ppm) signals.

**Synthesis of poly(pentyl malonate) (PPM).** In a glovebox, titanium isopropoxide (60  $\mu\text{L}$ , 0.2 mmol) were placed in a 100 mL round bottom flask equipped with a magnetic stir bar. Dimethyl malonate (26.9 g, 204 mmol) was added, followed by the addition of 1,5-pentanediol (20.8 g, 200 mmol). The flask was equipped with a 6-inch air reflux condenser and heated open to air at 120 °C for 12 h. Methanol was formed and evaporated throughout the course of reaction. The reactor was kept at 120 °C and attached to moderate vacuum (250 mmHg) for 3 h followed by high vacuum (0.3 mmHg) for another 3 h. Finally, the reactor was kept at 150 °C and high vacuum (0.3 mmHg) for 12 h, resulting in a pale-yellow viscous polymer (33.6 g, 98% yield). The crude pale-yellow product was purified via precipitation method in methanol solvent after dissolving dichloromethane (DCM) solvent. The precipitated product was purified again via second precipitation in diethyl ether solvent after dissolving DCM. Finally, the purified product was dried in the vacuum oven at 60 °C overnight.  $^1\text{H}$  NMR (500 MHz,  $\text{CDCl}_3$ ):  $\delta$  4.13 (4H), 3.73 (-OCH<sub>3</sub> end group), 3.62 (-CH<sub>2</sub>OH end group), 3.36 (2H), 1.67 (4H), 1.41 (2H) ppm.  $M_n$  (NMR) = 12.9 kg/mol,  $M_w/M_n$  = 2.4.

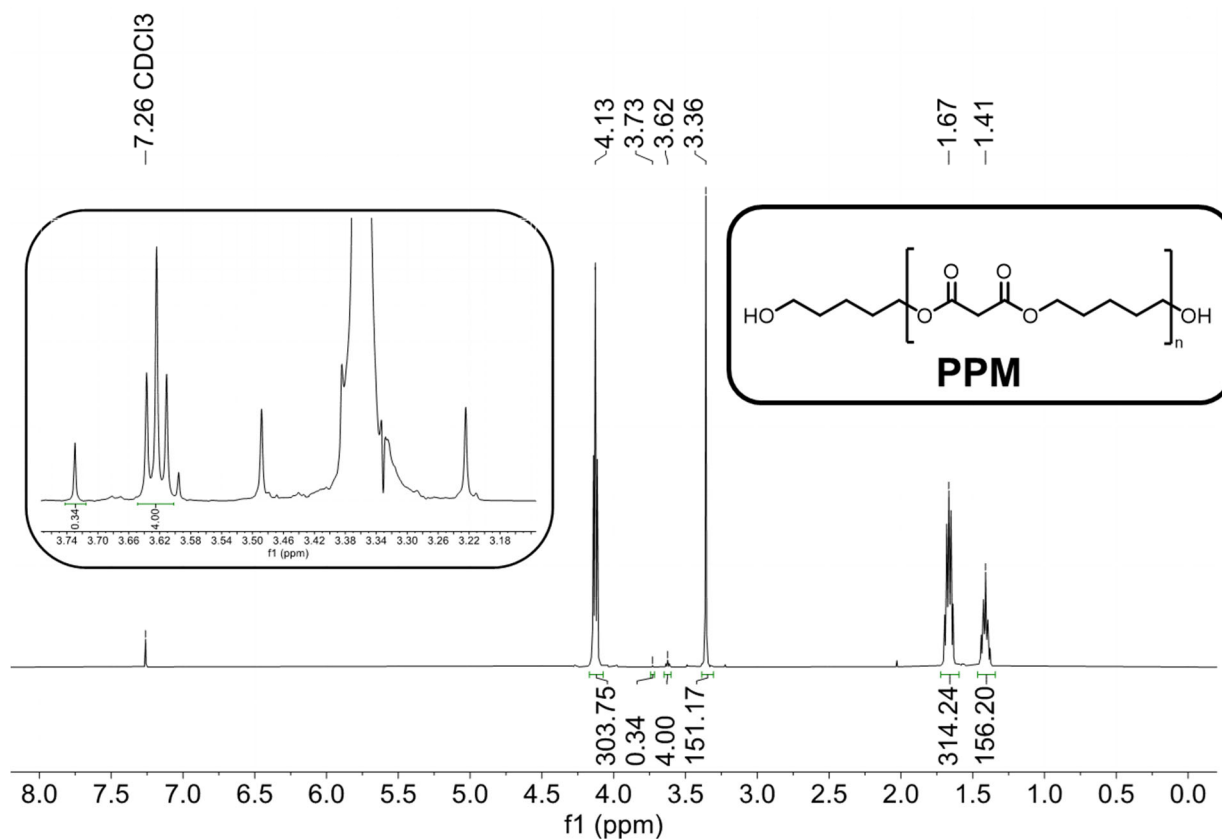


**Figure S1.**  $^1\text{H}$  NMR spectrum of poly(pentyl malonate) (PPM). The  $-\text{CH}_2\text{OH}$  (3.62 ppm) and  $-\text{OCH}_3$  (3.73 ppm) end group peaks are zoomed in for clarification. Most PPMs are  $-\text{CH}_2\text{OH}$  functionalized at both ends.

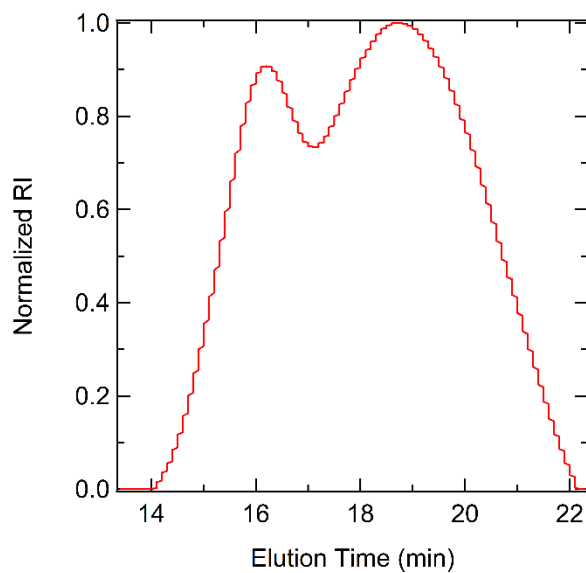


**Figure S2:** GPC trace of the PPM sample used in this study.

## S2. Gel Permeation Chromatography

PPM was characterized on an Agilent 1260 Infinity series GPC system. This system has Waters Styragel HR3 and HR4 columns with *N*-methyl-2-pyrrolidone (NMP) as the solvent. GPC was used to determine the molecular weight and polydispersity of the polymer. According to GPC, the PPM sample used in this study has a polydispersity ( $\bar{D}$ ) of 2.4 and a number-average molecular weight ( $M_n$ ) of 12.4 kg/mol. We do not expect the non-ideal molecular weight distribution of the sample to affect the sub-diffusive dynamics that are the focus of this paper. Previous studies has shown that the ion transport properties of polymers are independent of molecular weight.<sup>1</sup>

## S3. Polymer Electrolyte Preparation

Polymer electrolytes were prepared in an Argon filled glovebox to prevent water exposure to hygroscopic LiTFSI and PPM. Oxygen and water levels in the glovebox were kept below 1 ppm. PPM was dried under vacuum in the glovebox antechamber for 4 days at 90°C. Electrolytes were prepared in the glovebox by adding LiTFSI salt and PPM to a vial and adding approximately 15 mL of THF as a cosolvent. Vials were capped and agitated at approximately 60°C overnight to ensure complete dissolution of polymer and salt. The caps were then removed and left on the hot plate at 60°C for approximately 48 hours to evaporate off the majority of the solvent. In the final drying step, the electrolytes were placed under vacuum in the glovebox antechamber at 90°C for 4 days.

## S4. Electrochemical Properties of PPM Electrolyte

The electrochemical properties of PPM/LiTFSI mixtures are summarized in Refs. 2 and 3. The standard polymer electrolyte that has been studied extensively in the literature is pol(yethylene oxide) mixed with LiTFSI. In this section, we briefly summarize the data from these two systems at 90 °C. The limiting current,  $i_L$ , is defined as the maximum current that can be sustained in a cell containing the electrolyte of interest. This current is inversely proportional to the electrolyte thickness,  $L$ . It is therefore convenient to compare the thickness-normalized limiting current of different electrolytes,  $i_L L$ . In lithium-polymer-lithium cells,  $i_L L$  at  $r = 0.063$  of PEO/LiTFSI is 0.03 mA/cm while that of PPM/LiTFSI is 0.07 mA/cm. To our knowledge, the limiting current of PPM is the highest reported value for any polymer electrolyte in the literature.

Ion transport in any electrolyte with mobile cations and anions is governed by three transport properties. Two of these properties have been reported in the literature for PEO/LiTFSI and PPM/LiTFSI – conductivity and cation transference number.<sup>2, 3</sup> The conductivity of PEO/LiTFSI is higher than that of PPM/LiTFSI but the cation transference number of PPM/LiTFSI is higher than that of PEO/LiTFSI (see Refs. 2 and 3 for details). The main reason for the high limiting current in PPM/LiTFSI mixtures is cation transference.

## S5. QENS Sample Preparation

QENS samples were prepared using flat-plate aluminum cans provided by ORNL. Sample cans were placed flat on a hot plate and gently heated to 80°C. The polymer electrolyte was also heated to approximately 80°C until a single homogenous, bubble free layer within the can. Samples were then sealed using indium wire, and the lids were bolted on.

## S6. QENS Experiment

QENS measurements were taken at BASIS at Oak Ridge National Laboratory (ORNL). QENS measurements were taken for all samples at 30 K and 363 K. The magnitude of the scattering vector used to reduce the data is given by

$$Q = \left( \left( \frac{2\pi}{\lambda_i} \right)^2 + \left( \frac{2\pi}{\lambda_s} \right)^2 - 2 \left( \frac{2\pi}{\lambda_i} \right) \left( \frac{2\pi}{\lambda_s} \right) \cos\theta \right)^{\frac{1}{2}},$$

where  $\lambda_i$  and  $\lambda_s$  are the wavelengths of the incident and scattered neutrons, and  $\theta$  is the scattering angle. The  $Q$  values accessible at BASIS are between 0.3 and 1.9 Å<sup>-1</sup>. The BASIS instrument utilized Si(111) neutron-reflecting analyzer crystals, enabling access to energy transfers of ±100 μeV with an energy resolution of 3.6 μeV (full width at half maximum) and corresponding timescales between 0.02 and 1 nanoseconds. Because the difference between the incident and scattered wavelengths is small,  $Q$  is approximately given by

$$Q = \frac{4\pi}{\lambda_i} \sin\left(\frac{\theta}{2}\right).$$

The short-time limit of QENS instruments is governed by the maximum accessible energy transfer, while the long-time limit is governed by the minimum accessible energy transfer (the energy resolution). At BASIS, the maximum energy transfer accessible is defined by a combination of the neutron source frequency and the length of the spectrometer, while the minimum energy transfer

accessible is defined by a combination of the properties of the analyzer crystals and the length of the spectrometer. Scattering data was analyzed using the Mantid program (version 51) and corrected for empty cell contributions. Mantid 51 was also used to obtain the Fourier transform of the data.

The procedure for extracting the plateau value of the Rouse parameter from the QENS data in Figure 3a is as follows. For each data set at a given salt concentration, we first group five consecutive data points. Next, we calculate the mean value and the mean squared deviation for the data points within each group. Finally, we select the group with the smallest mean squared deviation, and its mean value is considered as the plateau value. The extracted plateau values along with the corresponding time regimes for selected groups are given in Table S1 for each salt concentration.

**Table S1.** Extracted plateau values and corresponding time regimes

$r$	$t_{start}$ (ns)	$t_{end}$ (ns)	Plateau value ( $\text{Log}_{10}(\langle r_d^2 \rangle / t^{\frac{1}{2}} / [\text{\AA}^2 / \text{ns}^{\frac{1}{2}}])$ )
0	0.3309	0.4963	1.4919
0.01	0.2481	0.4136	1.4405
0.02	0.2481	0.4136	1.3866
0.04	0.2895	0.4549	1.2984
0.06	0.4136	0.5790	1.2311
0.08	0.4136	0.5790	1.1821
0.10	0.4549	0.6203	1.1315

## S7. MD Simulation

MD simulation system consists of PPM polymer and LiTFSI salt. PPM polymer used in the simulation has a molecular weight of 2.6 kg/mol, which corresponds to 15 monomer units on each chain. The number of PPM polymer was kept at 25. The number of LiTFSI salt was adjusted from 0 to 150 as salt concentration,  $r$ , defined as the ratio between the number of  $\text{Li}^+$  and oxygen atoms from PPM polymer, increases from 0 to 0.1. The simulation box sizes ranges from 4.66 nm to 5.14 nm.

PPM polymer and LiTFSI salt were modeled based on the OPLS-AA force field.<sup>4,5</sup> The original OPLS-AA parameters, including the Lennard Jones (LJ) potentials, partial atomic charges, and bonded interactions were directly applied to LiTFSI salt. While the original LJ parameters and bonded interactions were adopted for PPM polymer, partial atomic charges were separately fitted as described in Ref. <sup>3</sup>. The simulations were performed at an elevated temperature of 430 K to account for the glass transition temperature difference between simulation and experiment.<sup>3</sup>

MD simulation was performed using the Gromacs package (version 5.1.4).<sup>6</sup> The Lorentz–Berthelot combination rule is used to obtain the LJ parameters between dissimilar atoms. The bonds involving hydrogen atoms were constrained using the LINCS algorithm.<sup>7</sup> An  $NpT$  ensemble with velocity-rescale thermostat<sup>8</sup> and Berendsen barostat<sup>9</sup> is implemented at 430 K and 1 bar. A global cutoff of 1.2 nm is used for computing LJ potential. The particle mesh Ewald (PME) method<sup>10</sup> was used to calculate the electrostatic interactions. A time step size of 2 fs was used. The simulation systems were first packed and energy minimized. Then, the systems were well mixed by performing a set of equilibrium simulations for 2 ns: (550 K, 1 bar), (500 K, 100 bar), (550 K, 100 bar), and (500 K, 1 bar). Next, the systems were further cooled and heated between (500 K, 1 bar) and (430 K, 1 bar) for three cycles. Finally, equilibrium simulations at (430 K, 1 bar) were performed for 200 ns at each salt concentration.

## S8. Lithium Solvation by PPM

The cutoff distance to determine whether a monomer coordinates  $\text{Li}^+$  is obtained from the radial distribution function between  $\text{Li}^+$  and oxygen from PPM. As shown in Figure S3, the coordination of  $\text{Li}^+$  by backbone oxygen on PPM is negligible compared with that from carbonyl oxygen. The position of the valley beyond the first peak is at  $r_d = 0.34$  nm, which is taken as the cutoff distance to determine whether a carbonyl oxygen coordinates a  $\text{Li}^+$ .

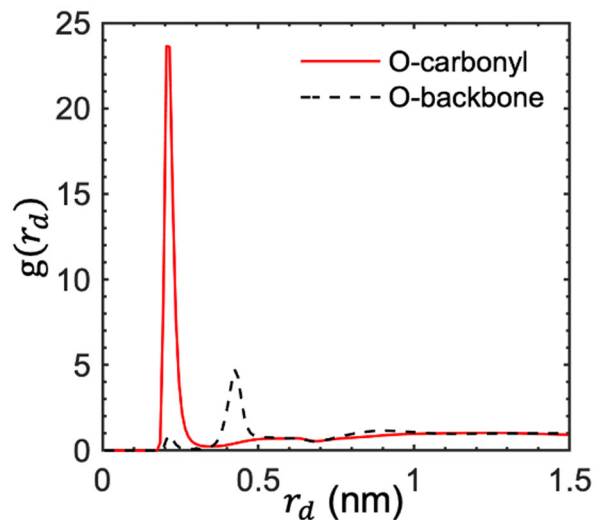


**Figure S3.** Radial distribution function between  $\text{Li}^+$  and oxygen atoms (both carbonyl oxygen and backbone oxygen) from PPM polymer at  $r = 0.10$ .

### S9. Contribution of Different Types of Hydrogens to Segmental Motion

The contribution of different types of hydrogens to segmental motion was disentangled via simulation. Figure S4 examines the MSDs of hydrogens located between two neighboring carbonyl groups and on the pentyl groups. Within the timescale of interest (0.1 to 10 ns), the two MSDs are quantitatively similar to the MSD averaged from all hydrogens on the chain. Therefore, our QENS results are not affected by deuteration of different types of hydrogens.

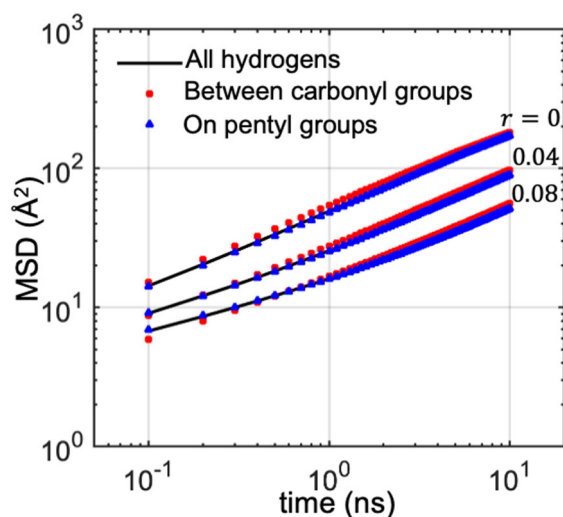


**Figure S4.** Comparison of MSDs of different types of hydrogens on the PPM chains at three salt concentrations. The hydrogens on the PPM chains are disentangled into two groups: those between two neighboring carbonyl groups and those on the pentyl chain.

### S10. Effect of Chain Length on Solvation Lifetime

Simulations were repeated for PPM/LiTFSI with different number of monomers ( $N_{mono}$ ) at a salt concentration of  $r = 0.10$ . The results in the main text are based on  $N_{mono} = 15$ ; the shortest chain consists of 3 monomers as the force field for PPM chain was developed for  $N_{mono} \geq 3$ .<sup>3</sup> As shown in Figure S5,  $\tau_s$  increases with chain length when  $N_{mono}$  is small and reaches a plateau when  $N_{mono}$  exceeds 6.  $\tau_s$  was also extrapolated to  $N_{mono} = 1$  (*i.e.*, the systems only consists of monomers of PPM and LiTFSI), which is 0.22 ns.

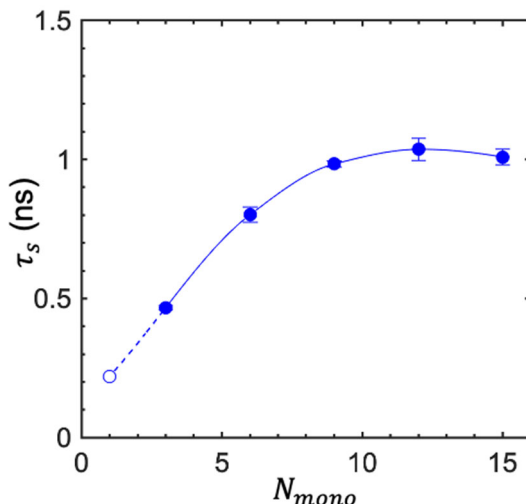


**Figure S5.** Effect of chain length on solvation lifetime at  $r = 0.10$ . Closed circles are data directly obtained from simulation, which were interpolated in the regime  $1 \leq N_{mono} \leq 15$ . The interpolation gives extrapolated values for  $1 \leq N_{mono} < 3$ , which are presented by open circles and dashed line as extrapolated values. Data are presented as mean values from four independent simulations and error bars denote the standard deviation.

### S11. Impact of Temperature on Solvation Lifetime

Simulations were performed at different temperatures for the  $N_{mono} = 9$  electrolyte at a salt concentration of  $r = 0.10$ . As shown in Figure S6,  $\tau_s$  shows an exponential decrease with increasing temperature. Therefore, the ultraslow process we have studied in the nonaqueous electrolyte will be even slower as compared to aqueous electrolyte at room temperature.

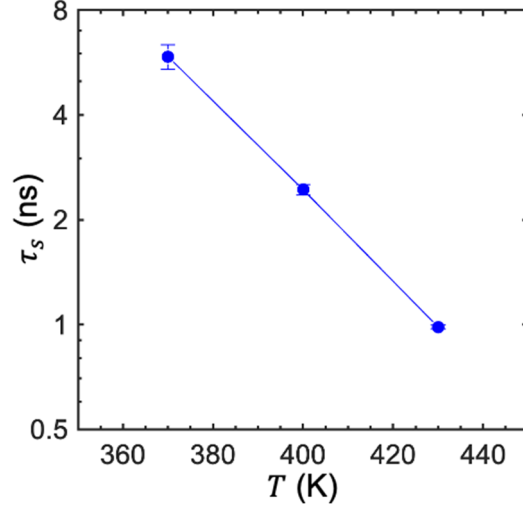


**Figure S6.** Impact of temperature on solvation lifetime for the  $N = 9$  electrolyte for  $r=0.1$ . Data are presented as mean values from four independent simulations and error bars denote the standard deviation.

## S12. Rouse Mode Analysis

The Rouse modes of a polymer chain with a length of  $N + 1$  are<sup>11, 12</sup>

$$\mathbf{X}_p(t) = \frac{1}{N+1} \sum_{n=1}^{N+1} \mathbf{R}_n \cos \left[ \frac{p\pi}{N+1} \left( n - \frac{1}{2} \right) \right], \quad (\text{S1})$$

where  $\mathbf{R}_n$  is the position of  $n$ th segment and  $p = 1, 2, \dots, N$  is the mode number. Each PPM monomer is taken as segment. Relaxation of the entire chain is described by  $p = 1$  mode, whereas  $p > 1$  mode describes the internal relaxation of a sub-chain consisting of  $N/p$  consecutive segments. The relaxation time of each mode ( $\tau_{R,p}$ ) describes the exponential decay of the autocorrelation  $\langle \mathbf{X}_p(t) \cdot \mathbf{X}_p(0) \rangle = \langle X_p^2 \rangle \exp(-t/\tau_{R,p})$  for an ideal chain. Figure S7a shows the autocorrelation functions at different modes obtained from the simulation for the PPM/salt system with  $r = 0.08$ . The relaxation times in simulations are usually better fitted through a stretched exponential function as  $\langle X_p^2 \rangle \exp \left[ (-t/\tau'_p)^{\beta_p} \right]$ ,<sup>13, 14</sup> and then the effective relaxation time of mode  $p$  is obtained by

$$\tau_{R,p} = \int_0^\infty \exp \left[ \left( -\frac{t}{\tau'_p} \right)^{\beta} \right] dt = \frac{\tau'_p}{\beta_p} \Gamma(1/\beta_p), \quad (\text{S2})$$

where  $\Gamma$  is the Gamma function. Figure S7b shows the corresponding relaxation times as a function mode number  $p$ . The fastest relaxation time  $\tau_{R,N}$  is found to be close to  $\tau_2$ . The longest relaxation time is obtained when  $p=1$ . The standard Rouse model indicates that  $\tau_{R,p} \propto 1/p^2$ .<sup>11</sup> The average number of monomers per chain in the PPM sample is 72. For the PPM/LiTFSI with a segmental

relaxation time of about 1 ns, we estimate the timescale for molecular relaxation based on the Rouse model to be about 5000 ns.

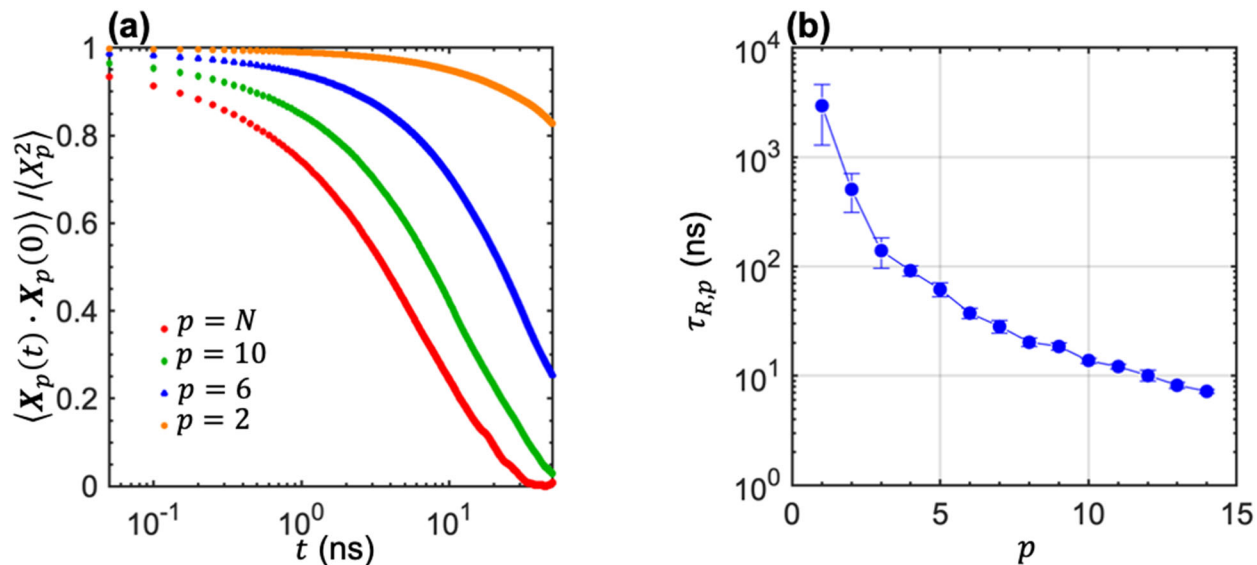


**Figure S7.** Rouse relaxation modes at  $r = 0.08$ . **(a)** The autocorrelation function for different modes. **(b)** The relaxation times ( $\tau_{R,p}$ ) as a function of mode number  $p$ .  $\tau_{R,p}$  are presented as mean values from four independent simulations and error bars denote the standard deviation.

## References

1. Gao, K. W.; Balsara, N. P., Electrochemical properties of poly (ethylene oxide) electrolytes above the entanglement threshold. *Solid State Ion.* **2021**, *364*, 115609.
2. Yu, X.; Hoffman, Z. J.; Lee, J.; Fang, C.; Gido, L. A.; Patel, V.; Eitouni, H. B.; Wang, R.; Balsara, N. P., A Practical Polymer Electrolyte for Lithium and Sodium Batteries: Poly (pentyl malonate). *ACS Energy Lett.* **2022**, *7* (11), 3791-3797.
3. Fang, C.; Yu, X.; Chakraborty, S.; Balsara, N. P.; Wang, R., Molecular Origin of High Cation Transference in Mixtures of Poly (pentyl malonate) and Lithium Salt. *ACS Macro Lett.* **2023**, *12*, 612-618.
4. Jorgensen, W. L.; Maxwell, D. S.; Tirado-Rives, J., Development and testing of the OPLS all-atom force field on conformational energetics and properties of organic liquids. *J. Am. Chem. Soc.* **1996**, *118* (45), 11225-11236.
5. Sambasivarao, S. V.; Acevedo, O., Development of OPLS-AA force field parameters for 68 unique ionic liquids. *J. Chem. Theory Comput.* **2009**, *5* (4), 1038-1050.
6. Abraham, M. J.; Murtola, T.; Schulz, R.; Páll, S.; Smith, J. C.; Hess, B.; Lindahl, E., GROMACS: High performance molecular simulations through multi-level parallelism from laptops to supercomputers. *SoftwareX* **2015**, *1*, 19-25.
7. Hess, B.; Bekker, H.; Berendsen, H. J.; Fraaije, J. G., LINCS: a linear constraint solver for molecular simulations. *J. Comput. Chem.* **1997**, *18* (12), 1463-1472.
8. Bussi, G.; Donadio, D.; Parrinello, M., Canonical sampling through velocity rescaling. *J. Chem. Phys.* **2007**, *126* (1), 014101.
9. Berendsen, H. J.; Postma, J. v.; Van Gunsteren, W. F.; DiNola, A.; Haak, J. R., Molecular dynamics with coupling to an external bath. *J. Chem. Phys.* **1984**, *81* (8), 3684-3690.
10. Darden, T.; York, D.; Pedersen, L., Particle mesh Ewald: An  $N \cdot \log(N)$  method for Ewald sums in large systems. *J. Chem. Phys.* **1993**, *98* (12), 10089-10092.
11. Doi, M.; Edwards, S. F., *The theory of polymer dynamics*. oxford university press: 1988; Vol. 73.
12. Kopf, A.; Dünweg, B.; Paul, W., Dynamics of polymer “isotope” mixtures: Molecular dynamics simulation and Rouse model analysis. *J. Chem. Phys.* **1997**, *107* (17), 6945-6955.
13. Shaffer, J. S., Effects of chain topology on polymer dynamics: Configurational relaxation in polymer melts. *J. Chem. Phys.* **1995**, *103* (2), 761-772.
14. Padding, J. T.; Briels, W. J., Time and length scales of polymer melts studied by coarse-grained molecular dynamics simulations. *J. Chem. Phys.* **2002**, *117* (2), 925-943.